Analysis of reinforced and thin-walled structures by multi-line refined 1D/beam models

Terms of use:

Publisher copyright

(Article begins on next page)

19 April 2024

Analysis of Reinforced and Thin-walled Structures by Multi-line Refined 1D/Beam Models

E. Carrera[ab]*, A. Pagani[a]†

[a]Department of Mechanical and Aerospace Engineering, Politecnico di Torino
Corso Duca degli Abruzzi 24, 10129 Torino, Italy.

[b]King Abdulaziz University, Jeddah, Saudi Arabi.

Author for correspondence:
E. Carrera, Professor of Aerospace Structures and Aeroelasticity
Department of Mechanical and Aerospace Engineering
Politecnico di Torino
Corso Duca degli Abruzzi 24
10129 Torino, Italy
tel: +39 011 090 6836
fax: +39 011 090 6899
e-mail: erasmo.carrera@polito.it

---

*Professor of Aerospace Structures and Aeroelasticity, e-mail: erasmo.carrera@polito.it
†Ph.D. student, e-mail: alfonso.pagani@polito.it

Abstract

This paper focuses the attention on the use of appropriate combinations of refined one-dimensional (1D) beam theories to analyze thin-walled, reinforced structures. The cross-section of a slender body is seen as the sum of different sub-domains. Each sub-domain is subsequently used as the cross-section of a beam discretization. Displacement variables are then expanded around the beam axis of each sub-domain by using refined 1D models which are based on the Carrera Unified Formulation. The order of the beam elements can vary in different sub-domains. This subdivision has been called "multi-line" as opposed to the "one-line" approach of classical beam theories. 1D compatibility conditions of the displacements at selected points of the sub-domain interface boundaries are imposed by using Lagrange multipliers. Various problems have been analyzed to highlight the advantages and disadvantages of the present multi-line approach. It is concluded that the multi-line approach appears very effective in the case of thin-walled sections made by locally connected walls as well as in the case of reinforced structures.

Keywords: Unified formulation; Higher-order theories; Beams; Reinforced Structures; Multi-line

1 Introduction

Beam models are widely used to analyze the mechanical behavior of slender bodies, such as columns, rotor-blades, aircraft wings, towers and bridges amongst others. The ease of application of one-dimensional (1D) theories and their computational efficiency are some of the main reasons why structural analysts prefer them to two-dimensional (2D) and three-dimensional (3D) models.

The classical and best-known beam theories are those by Euler [1] (hereinafter referred to as EBBM) and Timoshenko [2, 3] (hereinafter referred to as TBM). The former does not account for transverse shear deformations and rotatory inertia, whereas the latter assumes a uniform shear distribution along the cross-section of the beam together with the effects of rotatory inertia. These models yield reasonably good results when slender, solid section, homogeneous structures are subjected to flexure. Conversely, the analysis of deep, thin-walled, open section beams may require more sophisticated theories to achieve sufficiently accurate results (see [4]).

Over the last century, many refined beam theories have been proposed to overcome the limitation of classical beam modelling. Different approaches have been used to improve the beam models, which include the introduction of shear correction factors, the use of warping functions based on de Saint-Venant's solution, the variational asymptotic solution (VABS), the generalized beam theory (GBT), and others. Some selected references and noteworthy contributions are briefly discussed below.

Early investigators have focused on the use of appropriate shear corrections factors to increase the accuracy of classical 1D formulations, such as Timoshenko and Goodier [5], Sokolniko [6], Stephen [7], and Hutchinson [8]. The shear correction factor has generally been used as a static concept which is restrictive. In this respect, Jensen [9] showed how the shear correction factor can vary with the natural frequencies. Furthermore, a review paper by Kaneko [10] and a recent paper by Dong et al. [11] have highlighted the difficulty in the definition of a universally accepted formulation for shear correction factors.

Another important class of refinement methods in the literature is based on the use of warping functions. The contributions by El Fatmi [12, 13, 14] and Ladevéze et al. [15, 16] are some excellent examples.

Asymptotic type expansion in conjunction with variational methods has also been proposed; see for example Berdichevsky et al. [17], which also includes a commendable review of previous works on beam theory development. Some further valuable contributions have been made by Volovoi [18], Popescu and Hodges [19], Yu et al. [20], Yu and Hodges [21, 22].

GBT probably originated from the work of Schardt [23, 24]. GBT improves classical theories by using piece-wise beam description of thin-walled sections. It has been widely employed and extended in various forms by Silvetre et al. [25, 26, 27].

Higher-order theories are generally obtained by using refined displacement fields of the beam cross-sections. Washizu [28] ascertained how the use of an arbitrarily chosen rich displacement fields can lead to closed form exact 3D solutions. However, when complex cross-sections are considered, the solution becomes increasingly inaccurate as the distance from the reference axis of the beam increases.

To overcome this limitation of higher-order models, Multi-Line (ML) beam models are introduced in this paper. In the ML beam modelling approach, a slender body is discretized by means of multiple beam axes which are placed in different regions over the problem domain. 1D higher-order finite elements are developed within the framework of the Carrera Unified Formulation (CUF), which has been well established in the literature for over a decade [29, 30, 31, 32]. CUF is a hierarchical formulation that considers the order of the model N as a free-parameter (i.e. as input) of the analysis. In other words, refined models are obtained without the need for any ad hoc formulations. In the present work, beam theories using CUF are obtained on the basis of Taylor-type expansions (TE). EBBM and TBM can be obtained as particular or special cases. The strength of CUF TE 1D models in dealing with arbitrary geometries, thin-walled structures and identifying local effects is well known for both static [33, 34] and free-vibration analysis [35, 36, 37].

Different-order refined beam elements can be adopted for each beam-line in ML models. Then, once each beam axis has been discretized with 1D elements, Lagrange multipliers are used to impose constraints on displacement variables at a number of *connecting points* at the interface boundaries between each beam-line. The number of beam-lines and the order of the beam elements used to discretize each beam-line, as well as the number and the location of *connecting points* at the boundary interfaces, are all parameters of the ML model.

In the next section a brief overview of CUF is provided. Subsequently, the use of Lagrange multipliers for the development of ML models is described. Then, numerical results concerning reinforced and thin-walled structures are presented and the main conclusions are outlined.

2 Higher-order beam formulation

2.1 Preliminaries

The adopted rectangular cartesian coordinate system is shown in Fig. 1. Let us introduce the transposed displacement vector,

$$\mathbf{u}(x,y,z) = \left\{ \begin{array}{ccc} u_x & u_y & u_z \end{array} \right\}^T \tag{1}$$

The cross-sectional plane of the structure is denoted by Ω, and the beam boundaries over y are $0 \leq y \leq L$. The stress, $\boldsymbol{\sigma}$, and strain, $\boldsymbol{\epsilon}$, components are grouped as follows:

$$\begin{aligned}
\boldsymbol{\sigma}_p &= \left\{ \begin{array}{ccc} \sigma_{zz} & \sigma_{xx} & \sigma_{zx} \end{array} \right\}^T, & \boldsymbol{\epsilon}_p &= \left\{ \begin{array}{ccc} \epsilon_{zz} & \epsilon_{xx} & \epsilon_{zx} \end{array} \right\}^T \\
\boldsymbol{\sigma}_n &= \left\{ \begin{array}{ccc} \sigma_{zy} & \sigma_{xy} & \sigma_{yy} \end{array} \right\}^T, & \boldsymbol{\epsilon}_n &= \left\{ \begin{array}{ccc} \epsilon_{zy} & \epsilon_{xy} & \epsilon_{yy} \end{array} \right\}^T
\end{aligned} \tag{2}$$

In the case of small displacements with respect to a characteristic dimension in the plane of Ω, the strain - displacement relations are

$$\begin{aligned}
\boldsymbol{\epsilon}_p &= \mathbf{D}_p \mathbf{u} \\
\boldsymbol{\epsilon}_n &= \mathbf{D}_n \mathbf{u} = (\mathbf{D}_{n\Omega} + \mathbf{D}_{ny}) \mathbf{u}
\end{aligned} \tag{3}$$

where $\mathbf{D}_p$ and $\mathbf{D}_n$ are linear differential operators and the subscript "n" stands for terms lying on the cross-section, while "p" stands for terms lying on planes which are orthogonal to Ω.

$$\mathbf{D}_p = \begin{bmatrix} 0 & 0 & \frac{\partial}{\partial z} \\ \frac{\partial}{\partial x} & 0 & 0 \\ \frac{\partial}{\partial z} & 0 & \frac{\partial}{\partial x} \end{bmatrix}, \quad \mathbf{D}_{n\Omega} = \begin{bmatrix} 0 & \frac{\partial}{\partial z} & 0 \\ 0 & \frac{\partial}{\partial x} & 0 \\ 0 & 0 & 0 \end{bmatrix}, \quad \mathbf{D}_{ny} = \begin{bmatrix} 0 & 0 & \frac{\partial}{\partial y} \\ \frac{\partial}{\partial y} & 0 & 0 \\ 0 & \frac{\partial}{\partial y} & 0 \end{bmatrix} \tag{4}$$

Constitutive laws are now exploited to obtain stress components to give

$$\boldsymbol{\sigma} = \tilde{\mathbf{C}} \boldsymbol{\epsilon} \tag{5}$$

Equation (5) can be split into $\boldsymbol{\sigma}_p$ and $\boldsymbol{\sigma}_n$ with the help of Eq. (2) so that

$$\begin{aligned}
\boldsymbol{\sigma}_p &= \tilde{\mathbf{C}}_{pp} \boldsymbol{\epsilon}_p + \tilde{\mathbf{C}}_{pn} \boldsymbol{\epsilon}_n \\
\boldsymbol{\sigma}_n &= \tilde{\mathbf{C}}_{np} \boldsymbol{\epsilon}_p + \tilde{\mathbf{C}}_{nn} \boldsymbol{\epsilon}_n
\end{aligned} \tag{6}$$

The matrices $\tilde{\mathbf{C}}_{pp}$, $\tilde{\mathbf{C}}_{nn}$, $\tilde{\mathbf{C}}_{pn}$, and $\tilde{\mathbf{C}}_{np}$ are explicitly given in [32] and they contain the material coefficients.

Within the framework of CUF, the displacement field $\mathbf{u}(x, y, z)$ can be expressed as

$$\mathbf{u}(x, y, z) = F_\tau(x, z)\mathbf{u}_\tau(y), \qquad \tau = 1, 2, ..., M \tag{7}$$

where F_τ are the functions of the coordinates x and z on the cross-section. $\mathbf{u}_\tau$ is the vector of the *generalized* displacements, M stands for the number of terms used in the expansion, and the repeated subscript, τ, indicates summation. The choice of F_τ determines the class of the 1D CUF model that is required and subsequently to be adopted. TE (Taylor expansion) 1D CUF models - described by Eq. (7) - consists of a Maclaurin series that uses the 2D polynomials $x^i\ z^j$ as base, where i and j are positive integers. For instance, the displacement field of the second-order $(N = 2)$ TE model can be expressed as

$$\begin{aligned}
u_x &= u_{x_1} + x\ u_{x_2} + z\ u_{x_3} + x^2\ u_{x_4} + xz\ u_{x_5} + z^2\ u_{x_6} \\
u_y &= u_{y_1} + x\ u_{y_2} + z\ u_{y_3} + x^2\ u_{y_4} + xz\ u_{y_5} + z^2\ u_{y_6} \\
u_z &= u_{z_1} + x\ u_{z_2} + z\ u_{z_3} + x^2\ u_{z_4} + xz\ u_{z_5} + z^2\ u_{z_6}
\end{aligned} \tag{8}$$

The order N of the expansion is set as an input option of the analysis; the integer N is arbitrary and defines the order the beam theory. The Timoshenko beam model (TBM) can be realised by using a suitable F_τ expansion. Two conditions have to be imposed: (1) a first-order $(N = 1)$ approximation kinematic field and (2) the displacement components u_x and u_z have to be constant above the cross-section. By contrast, the Euler-Bernoulli beam model (EBBM) can be obtained through the penalization of ϵ_{xy} and ϵ_{zy}. Classical theories and first-order models $(N = 1)$ require the necessary assumption of reduced material stiffness coefficients to correct Poisson's locking (see [38]). In this paper, Poisson's locking is corrected according to the method outlined by Carrera et al. [32]. A detailed description of TE CUF models can be found in [32].

2.2 Refined 1D finite elements

The FE approach is used to discretize the structure along the y-axis. This process is conducted via a classical finite element technique, where the displacement vector is given by

$$\mathbf{u}(x, y, z) = F_\tau(x, z)N_i(y)\mathbf{q}_{\tau i} \tag{9}$$

N_i stands for the shape functions and $\mathbf{q}_{\tau i}$ for the nodal displacement vector. For the sake of brevity, the shape functions are not reported here. They can be found in many books, for instance in [39]. Elements with four nodes (B4) are used in this work, that is, a cubic approximation along the y-axis is assumed. The choice of the theory order, N, is completely independent of the choice of the beam finite element to be used along the axis of the beam.

The principle of virtual displacements is used to derive the elemental stiffness matrix and the external loadings vector.

$$\delta L_{\text{int}} = \int_V (\delta \boldsymbol{\epsilon}_p^T \boldsymbol{\sigma}_p + \delta \boldsymbol{\epsilon}_n^T \boldsymbol{\sigma}_n)\, \mathrm{d}V = \delta L_{\text{ext}} \tag{10}$$

where L_{int} stands for the strain energy and L_{ext} is the work done by the external loadings. δ stands for the usual virtual variation operator. The virtual variation of the strain energy is rewritten using Eq.s (3), (6) and (9).

$$\delta L_{\text{int}} = \delta \mathbf{q}_{\tau i}^T \boldsymbol{K}^{ij\tau s} \mathbf{q}_{sj} \tag{11}$$

$\boldsymbol{K}^{ij\tau s}$ is the stiffness matrix in the form of the fundamental nucleus. In a compact notation, it can be written as

$$\begin{aligned}
\boldsymbol{K}^{ij\tau s} = \; & I_l^{ij} \triangleleft \left(\boldsymbol{D}_{np}^T F_\tau \boldsymbol{I}\right)\left[\tilde{\boldsymbol{C}}_{np}\left(\boldsymbol{D}_p F_s \boldsymbol{I}\right) + \tilde{\boldsymbol{C}}_{nn}\left(\boldsymbol{D}_{np} F_s \boldsymbol{I}\right)\right] + \\
& \left(\boldsymbol{D}_p^T F_\tau \boldsymbol{I}\right)\left[\tilde{\boldsymbol{C}}_{pp}\left(\boldsymbol{D}_p F_s \boldsymbol{I}\right) + \tilde{\boldsymbol{C}}_{pn}\left(\boldsymbol{D}_{np} F_s \boldsymbol{I}\right)\right] \triangleright_\Omega + \\
& I_l^{ij,y} \triangleleft \left[\left(\boldsymbol{D}_{np}^T F_\tau \boldsymbol{I}\right)\tilde{\boldsymbol{C}}_{nn} + \left(\boldsymbol{D}_p^T F_\tau \boldsymbol{I}\right)\tilde{\boldsymbol{C}}_{pn}\right] F_s \triangleright_\Omega \boldsymbol{I}_{\Omega y} + \\
& I_l^{i,y j} \boldsymbol{I}_{\Omega y} \triangleleft F_\tau \left[\tilde{\boldsymbol{C}}_{np}\left(\boldsymbol{D}_p F_s \boldsymbol{I}\right) + \tilde{\boldsymbol{C}}_{nn}\left(\boldsymbol{D}_{np} F_s \boldsymbol{I}\right)\right] \triangleright_\Omega + \\
& I_l^{i,y j,y} \boldsymbol{I}_{\Omega y} \triangleleft F_\tau \tilde{\boldsymbol{C}}_{nn} F_s \triangleright_\Omega \boldsymbol{I}_{\Omega y}
\end{aligned} \tag{12}$$

where

$$\boldsymbol{I}_{\Omega y} = \begin{bmatrix} 0 & 1 & 0 \\ 1 & 0 & 0 \\ 0 & 0 & 1 \end{bmatrix} \qquad \triangleleft \ldots \triangleright_\Omega = \int_\Omega \ldots \, d\Omega \tag{13}$$

$$\left(I_l^{ij}, I_l^{ij,y}, I_l^{i,y j}, I_l^{i,y j,y}\right) = \int_l \left(N_i N_j, N_i N_{j,y}, N_{i,y} N_j, N_{i,y} N_{j,y}\right) dy \tag{14}$$

It should be noted that $\boldsymbol{K}^{ij\tau s}$ does not depend either on the expansion order or on the choice of the F_τ expansion polynomials. These are the key-points of CUF which allows, with only nine FORTRAN statements, the implementation of any-order of multiple class theories.

For the sake of brevity, the derivation of the loading vector from the virtual variation of the work

7

of external loadings, δL_ext, is not provided in this paper. It can be found in [32] for different loading conditions.

3   Multi-line refined beam models

The method of Lagrange multipliers provides the stationary conditions of a constrained functional. The application of Lagrange multipliers to CUF has recently been introduced in [40], where Lagrange multipliers are used to implement higher-order 1D models with variable kinematic field along the beam axis. A more generic discussion of the Lagrange multipliers method can be found in [41, 42], whereas Zienkiewicz and Taylor [43] show the use of multipliers in Finite Element Method (FEM) for contact and tied interfaces, for multibody coupling and to avoid the necessity of C^1 continuity for the problem of thin plates.

In the present paper, Lagrange multipliers are used to implement ML models. In Fig. 2a a slender structure discretized by two different beam axes is shown. Higher-order elements of arbitrary order are placed on each beam-line, which separately describes a given sub-region of the whole structure. Lagrange multipliers are then used to impose compatibility on displacement variables at a number of *connecting points* at the interface boundary between beam-lines.

If we consider two points, 1 and 2, sharing the same position on the interface boundary, the *Lagrangian* that has to be added to the original problem in order to impose the equality of displacements is

$$\Pi = \boldsymbol{\lambda}^T\left(\mathbf{u}^1 - \mathbf{u}^2\right) \tag{15}$$

where $\mathbf{u}^1$ and $\mathbf{u}^2$ are the displacements of points 1 and 2, respectively. Points 1 and 2 belong to different beam-lines. $\boldsymbol{\lambda}$ is the vector containing the Lagrange multipliers. Equation (15) is rewritten in terms of CUF with the help of Eq. (9).

$$\Pi = \boldsymbol{\lambda}^T\mathbf{B}\mathbf{q} \tag{16}$$

where the fundamental nucleus of the matrix $\mathbf{B}$ is

$$\mathbf{B}^{\tau i} = \left(F_\tau^1 N_i^1 - F_\tau^2 N_i^2\right)\mathbf{I} \tag{17}$$

$\mathbf{I}$ is the identity matrix with dimensions 3×3. $F_\tau^1 N_i^1$ and $F_\tau^2 N_i^2$ are the products of the cross-sectional functions of Eq. 7 and the shape functions along the beam axis computed at points 1 and

2, respectively. The superscripts "1" and "2" also denote the fact that, generally, different beam axes can be modeled with different beam theories. More details about the use of multipliers in refined beam theories can be found in [40].

The solution of the problem is given by finding $\mathbf{q}$ and $\boldsymbol{\lambda}$ from the following linear system:

$$
\begin{cases}
\mathbf{Kq} + \dfrac{\partial \Pi}{\partial \mathbf{q}} &= \mathbf{F} \\
\dfrac{\partial \Pi}{\partial \boldsymbol{\lambda}} &= \overline{\mathbf{u}}
\end{cases}
\tag{18}
$$

where $\mathbf{F}$ is the loadings vector and $\overline{\mathbf{u}}$ is equal to 0 for homogeneous conditions. $\mathbf{K}$ is the global stiffness matrix. $\mathbf{K}$ is built by assembling the stiffness matrices of each beam-line - which are computed according to the previous section - as shown in Fig. 2b. Equation (18) is rewritten using Eq. (16). In a matrix form it reads

$$
\begin{bmatrix} \mathbf{K} & \mathbf{B}^T \\ \mathbf{B} & 0 \end{bmatrix} \begin{bmatrix} \mathbf{q} \\ \boldsymbol{\lambda} \end{bmatrix} = \begin{bmatrix} \mathbf{F} \\ 0 \end{bmatrix}
\tag{19}
$$

The use of the multipliers method offers many advantages. However, the main disadvantage of its use in structural problems is that the matrix of Eq. (19) is not, in general, positive definite.

4 Numerical Results

In this section the accuracy and computational efficiency of the present higher-order ML models are demonstrated by carrying out the static analysis of both reinforced and thin-walled structures and the results are presented. First, the analysis of a beam with a I-shaped cross-section is discussed so as to make an easy and straightforward comparison with classical beam theories. Next, a reinforced thick plate undergoing a bending-torsional loading condition is considered. A thin-walled beam with a circular cross-section is subsequently analyzed to highlight the usefulness of the higher-order terms in the detection of in-plane deformations. Finally, a riveted structure is used to show the capability of the present ML models to take into account the effects due to localized constraints such as mechanical fasteners and welded joints. ML solutions are compared with results by classical and higher-order single-line CUF theories together with the results obtained from the finite element commercial code MSC Nastran.

4.1 I-section beam

A cantilever beam with a I-shaped cross-section such as the one shown in Fig. 3 is considered first. It is assumed that the beam has a height $h = 100$ mm and a width $w = 96$ mm. The length to height ratio, L/h, is 10. The thickness of the flanges is $t_1 = 8$ mm, whereas the thickness of the web is $t_2 = 5$ mm. The material data are: elastic modulus $E = 200$ GPa and Poisson ratio, ν, equal to 0.29. A vertical force $F_z = -2 \times 10^3$ N is applied at point B (see Fig. 3) at the free end of the beam.

Table 1 shows the vertical displacements, u_z, at the tip of the beam, at points A and B, which are shown in Fig. 3. The number of the degrees of freedom (DOFs) is also given for each model in Table 1. The results are compared with 3D (Solid) and 2D (Shell) FEM solutions obtained using commercial code MSC Nastran. The Solid model was constructed by using 8-node CHEXA elements having approximately a unitary aspect ratio. On the other hand, the Shell model was obtained with 4-node CQUAD4 shell elements. In Table 1 the vertical displacement u_{z_B} by the Shell model is between brackets since it was measured on the midplane of the flange and not exactly at point B. The analytical result achieved through Euler-Bernoulli beam theory is also given for comparison purposes, $u_{z_b} = \frac{F_z L^3}{3EI}$, where I is the cross-section moment of inertia. The results by classical and refined CUF single-line models are shown in rows 6 to 15, where up to eight-order ($N = 8$) beam models are considered. The last rows of Table 1 give the results by the ML models of the I-section beam.

Figure 4 shows the difference between the single-line and the present ML models. In the single-line approach, 10 B4 refined beam elements are placed on one beam axis. Conversely, in the ML models of the I-shaped cross-section structure, three beam axes are used. Specifically, one beam-line is placed on the web and one beam-line is placed on each flange. 10 B4 beam elements are used for each beam-line. Compatibility of displacements is subsequently imposed at three points per beam node on the interfaces between flanges and web through Lagrange multipliers. Unlikely the problems discussed in [40] where the number of connecting points was chosen on the basis of a convergence study, for the present ML models it was found that the convergence of the solution is guarantee with a few connecting points. For this reason the attention is not focused on this problem in the present paper. The ML models of the I-section beam are referred to as ML_{N_f, N_w}, where N_f is the expansion order of the beam elements placed on beam-lines of the flanges and N_w is the expansion order of the beam elements placed on the beam-line of the web.

Figure 5 shows the deformation of the free end of the beam. ML models are compared to the eight-order single-line model and to the Solid model. Finally, Fig. 6 shows the distribution of normal

stresses, σ_{yy}, at the clamped end for different structural models. Based on these results the following comments can be made:

- Classical and higher-order single-line models cannot detect the warping due to the bending-torsional load according to MSC Nastran results.

- Lower-order elements can be effective when used in a ML approach. In fact, third-order ($ML_{3,3}$) and fourth-order ($ML_{4,2}$, $ML_{4,3}$, and $ML_{4,4}$) ML models match Shell and Solid solutions both in terms of displacement and stress fields.

- The number of the degrees of freedom of ML models is extremely reduced if compared to MSC Nastran and single-line refined models.

4.2 Reinforced plate

The analysis of a reinforced thick plate was carried out next. The cross-section of the beam is shown in Fig. 7 together with verification points, A and B. The main dimensions of the structure are also given in Fig. 7. The length of the beam along the y-axis was set to $L = 1$ m. The whole structure was made of a material with Young's modulus $E = 75$ GPa and Poisson's ratio $\nu = 0.3$. The beam was clamped at one end and loaded with a vertical load, $F_z = 100$ N, at point A on the free end.

Table 2 shows the vertical displacements, u_z, and normal stress components, σ_{yy}, at points A and B on free and clamped cross-sections, respectively. The number of DOFs is also quoted for each model. MSC Nastran models are given for comparison purposes. The Solid model was built with 8-node CHEXA elements as in the previous example. The Shell/Beam model was constructed by using a combination of shell and beam finite elements. Specifically, CQUAD4 shell elements were used to discretize the plate, whereas 2-node CBEAM 1D finite elements were used for the stringers. In the Shell/Beam model, particular attention was given to the introduction of fictitious offsets between the plate and the stringers. The results by the Shell/Beam model are given in brackets since they are measured on the mid-plane of the plane as close as possible to points A and B. Rows 5 to 15 show the results by classical and higher-order single-line CUF models. Up-to-ninth-order models are considered. Rows 18 to 23 show the results by ML models.

Some examples of ML modelling approaches to the analysis of the reinforced plate are outlined in Fig. 8. The three-line model (Fig. 8c) was considered in this paper and the results are given in Table 2. In the three-line model, one beam-line is used to model each component of the structure, i.e. the panel and the two stringers. Each stringer is then constrained at the panel by imposing

displacements equality at two points per beam node on the interface boundary. 10 B4 elements were used for each beam-line in the present analysis. This three-line model of the reinforced panel is referred to as ML_{N_p,N_s}, where N_p is the expansion order of the refined beam elements used to discretize the panel and N_s is the expansion order of the elements on the stringers.

Finally, Fig. 9 shows the normal stresses, σ_{yy}, distribution at the clamped cross-section. The following comments arise from the analysis:

- The use of refined theories appears to be mandatory to provide significant improvements in the prediction of the torsional structural behavior by means of beam modeling. In fact, high expansion orders are necessary to detect the bending-torsional behavior of the reinforced plate if single-line models are adopted.

- Lower-order elements can be effective if ML approach is used, as shown in the previous example. ML models of the reinforced panel give good results with a number of DOFs which is lower than MSC Nastran and single-line models.

- ML models represent a valid alternative for the analysis of reinforced structures, which are usually analysed by means of a combination of beam and shell finite elements.

4.3 Thin-walled cylinder

A cantilever thin-walled cylinder was considered. The cross-section geometry of the beam is shown in Fig. 10. The outer diameter, d, was set to 1 m, whereas the thickness, t, was 0.02 m. The length-to-diameter ratio, L/d, was taken to be equal to 10. The cylinder was made of the same material as in the previous example. A vertical load, $F_z = 10^3$ N, was applied at point A (see Fig. 10), at the free end.

Figure 11 shows the difference between single-line beam models and the ML models implemented. In particular, two- and four-line models were considered for the analysis. In the two-line model, the cylinder was separated into two independent caps. Each cap was then discretized with 1D higher-order elements. Subsequently, the two caps were constrained together by imposing displacements equality at two nodes on each interface boundary in correspondence of the beam nodes. The two-line models are hereafter referred to as $ML2_{N_t,N_b}$, where N_t is the expansion order of the beam elements laying in the top beam-line and N_b is the expansion order of the elements laying on the bottom beam-line. Similarly, the four-line models are composed by four distinct caps, each of which is discretized by a beam-line. The four-line models are hereafter referred to as $ML4_{N_t,N_b,N_l,N_r}$, where N_t, N_b, N_l,

and N_r are the expansion orders of the refined elements lying on the top, bottom, left, and right beam-line, respectively. 10 B4 beam elements were placed each beam-line of the ML models.

Table 3 compares the vertical displacements, u_z, at verification points on the tip cross-section for single- and multi-line CUF models to MSC Nastran solutions. Both solid and a shell FEM models are provided. As in the previous examples, MSC Nastran CHEXA finite elements were used for the development of the Solid FEM model, whereas CQUAD4 elements where used for the Shell model. Comparison of the normal stress, σ_{yy}, is shown in Tab. 4, where the results from both the present and reference models are given.

Figure 12 shows the in-plane deformation of the loaded cross-section at the tip of the beam. Both two- and four-line models are compared to classical (EBBM) and higher-order (N=11) beam models as well as to Shell model. The following statements are worthy of careful study:

- Very high expansion orders are needed to correctly detect the displacement field of the thin-walled cylinder undergoing a concentrated load.

- The eleventh-order ($N = 11$) single-line model provides good results if compared to the solution from the MSC Nastan model with a significant reduction of the computational effort.

- The results given by the multi-line models, such as the ML2$_{9,5}$ and the ML4$_{7,7,5,5}$ models, are in good agreement with reference results. However, no particular improvements in terms of computational efficiency are evident with respect to single-line models. This is mainly due to the continuous geometry of the structure considered.

4.4 Riveted I-section beam

Reinforced structures are rarely obtained through industrial extrusion processes. These kind of structures are more likely realized by assembling different components (i.e. flanges, plates, webs and stringers) by means of rivets, studs, or welded joints. One of the most important feature of the present ML approach is that it allows to take into account the effects of those local joints such as mechanical fasteners. In order to show this characteristic of ML models, the I-section beam addressed in the first example is here re-considered. For the I-shaped beam whose results are given in this section, the horizontal flanges and the vertical web were considered as separate components. As shown in Fig. 13, flanges and web were linked via stringers. Each stringer was constrained to the web and the flange by means of one (CASE A) or two (CASE B) rivets. The distance between two rivets in the y-axis direction is 31.25 mm.

The dimensions of the beam, i.e. the width w, the height h, the thicknesses t_1 and t_2, and the length L, were the same as in the first analysis case. The stringers had sides equal to $a = 15$ mm, as shown in Fig. 13, whereas their thickness was set equal to t_2. The structure was made of the same material as in the first example. The beam had clamped-free boundary conditions and it underwent a vertical point load, $F_z = -2 \times 10^3$ N, which was placed at the top left corner on the free end.

ML models of the riveted I-section beam were built with seven beam-lines, with 10 B4 elements each. Specifically, each component of the structure (i.e. flanges, web and stringers) was modelled by one beam-line. Subsequently, components were linked each other at boundary interfaces via Lagrange multipliers, which simulate the rivets. In the following, ML models of the riveted beam are referred to as $\mathrm{ML}_{N_f, N_w, N_s}$, where N_f, N_w, and N_s are the expansion orders of the refined beam elements discretizing the flanges, the web, and the stringers, respectively.

Table 5 shows the vertical displacement of the loaded point for both single- and multi-line 1D higher-order models. Several ML models were considered and the results of both CASE A and CASE B are given. The results by ML models are also compared to the solution from a solid model by MSC Nastran. 8-node CHEXA elements were used in the construction of the solid model and MSC Nastran rigid *Multipoint Constraints* (MPC) were used to simulate the rivets. Figure 14 shows the distribution of the displacement components, $\sqrt{u_x^2 + u_y^2 + u_z^2}$, on the free end of the beam from both ML, single-line, and Solid models. The following comments are valid:

- ML models give the possibility to simulate the effects due to mechanical fasteners on reinforced structures.

- ML models allow for the obtaining of 3D-like solutions with low computational efforts.

- The error committed by neglecting the effects of the rivets ranges from 14% (CASE B) to 30% (CASE A), as shown from the comparison between the ninth-order ($N = 9$) single-line model and the $\mathrm{ML}_{4,4,4}$ model.

5   Conclusions

A higher-order multi-line approach to the analysis of slender bodies has been presented in this paper. Refined beam elements have been formulated using CUF, which allows for the formulation of any-order beam theories by setting the expansion order as input of the analysis. Multiple beam axes discretizing the same structure have been coupled by imposing compatibility of displacements at

a number of *connecting points* at the boundary interface using Lagrange multipliers. The results agree with the models obtained using solid, shell, and beam finite elements by the commercial code MSC Nastran. The present method has shown to be highly efficient for the analysis of reinforced structures in which the cross-section is physically made by different components connected each others by mechanical fasteners or welded joints. On the other hand, the method does not introduce particular advantages for the analysis of continuous/compact structures. Future work could be aimed to the improvement of ML models by means of the impositions of more distributed constraints in integral form at boundary interfaces. Comparisons with results obtained by imposing conditions on strains at boundary interfaces would be of interest too. Moreover, the extension of these conditions to stresses would allow the application of the present ML models to laminated composites structures.

References

[1] L. Euler, De curvis elasticis, Lausanne and Geneva: Bousquet, 1744, (English translation: W. A. Oldfather, C. A. Elvis, D. M. Brown, Leonhard Euler's elastic curves, Isis 20 (1933) 72–160).

[2] S. P. Timoshenko, On the corrections for shear of the differential equation for transverse vibrations of prismatic bars, Philosophical Magazine 41 (1922) 744–746.

[3] S. P. Timoshenko, On the transverse vibrations of bars of uniform cross section, Philosophical Magazine 43 (1922) 125–131.

[4] V. V. Novozhilov, Theory of elasticity, Pergamon, Elmsford, 1961.

[5] S. P. Timoshenko, J. N. Goodier, Theory of elasticity, McGraw-Hill, 1970.

[6] I. S. Sokolnikoff, Mathematical theory of elasticity, McGraw-Hill, 1956.

[7] N. G. Stephen, Timoshenko's shear coefficient from a beam subjected to gravity loading, Journal of Applied Mechanics 47 (1980) 121–127.

[8] J. R. Hutchinson, Shear coefficients for Timoshenko beam theory, Journal of Applied Mechanics 68 (2001) 87–92.

[9] J. J. Jensen, On the shear coefficient in Timoshenko's beam theory, Journal of Sound and Vibration 87 (4) (1983) 621–635.

[10] T. Kaneko, On Timoshenko's correction for shear in vibrating beams, Journal of Physics D: Applied Physics 8 (1975) 1927–1936.

[11] S. B. Dong, C. Alpdongan, E. Taciroglu, Much ado about shear correction factors in Timoshenko beam theory, International Journal of Solids and Structures 47 (2010) 1651–1665.

[12] R. El Fatmi, On the structural behavior and the Saint Venant solution in the exact beam theory: application to laminated composite beams, Computers and Structures 80 (16–17) (2002) 1441–1456.

[13] R. El Fatmi, Non-uniform warping including the effects of torsion and shear forces. Part I: a general beam theory, International Journal of Solids and Structures 44 (18–19) (2007) 5912–5929.

[14] R. El Fatmi, Non-uniform warping including the effects of torsion and shear forces. Part II: analytical and numerical applications, International Journal of Solids and Structures 44 (18–19) (2007) 5930–5952.

[15] P. Ladévèze, J. Simmonds, New concepts for linear beam theory with arbitrary geometry and loading, European Journal Of Mechanics A/Solids 17 (3) (1998) 377–402.

[16] P. Ladévèze, P. Sanchez, J. Simmonds, Beamlike (Saint-Venant) solutions for fully anisotropic elastic tubes of arbitrary closed cross-section, International Journal of Solids and Structures 41 (7) (2004) 1925–1944.

[17] V. L. Berdichevsky, E. Armanios, A. Badir, Theory of anisotropic thin-walled closed-cross-section beams, Composites Engineering 2 (5–7) (1992) 411–432.

[18] V. V. Volovoi, D. H. Hodges, V. L. Berdichevsky, V. G. Sutyrin, Asymptotic theory for static behavior of elastic anisotropic I-beams, International Journal of Solids and Structures 36 (1999) 1017–1043.

[19] B. Popescu, D. H. Hodges, On asymptotically correct Timoshenko-like anisotropic beam theory, International Journal of Solids and Structures 37 (2000) 535–558.

[20] W. Yu, V. V. Volovoi, D. H. Hodges, X. Hong, Validation of the variational asymptotic beam sectional analysis (VABS), AIAA Journal 40 (2002) 2105–2113.

[21] W. Yu, D. H. Hodges, Elasticity solutions versus asymptotic sectional analysis of homogeneous, isotropic, prismatic beams, Journal of Applied Mechanics 71 (2004) 15–23.

[22] W. Yu, D. H. Hodges, Generalized Timoshenko theory of the variational asymptotic beam sectional analysis, Journal of the American Helicopter Society 50 (1) (2005) 46–55.

[23] R. Schardt, Eine erweiterung der technischen biegetheorie zur berechnung prismatischer faltwerke (Extension of the engineer's theory of bending to the analysis of folded plate structures), Der Stahlbau 35 (1966) 161–171.

[24] R. Schardt, Generalized beam theory an adequate method for coupled stability problems, Thin-Walled Structures 19 (1994) 161–180.

[25] N. Silvestre, D. Camotim, First-order generalised beam theory for arbitrary orthotropic materials, Thin-Walled Structures 40 (9) (2002) 755–789.

[26] N. Silvestre, Second-order generalised beam theory for arbitrary orthotropic materials, Thin-Walled Structures 40 (9) (2002) 791–820.

[27] N. Silvestre, Generalised beam theory to analyse the buckling behaviour of circular cylindrical shells and tubes, Thin-Walled Structures 45 (2) (2007) 185–198.

[28] K. Washizu, Variational Methods in Elasticity and Plasticity, Pergamon, Oxford, 1968.

[29] E. Carrera, A class of two dimensional theories for multilayered plates analysis, Atti Accademia delle Scienze di Torino, Memorie Scienze Fisiche 19-20 (1995) 49–87.

[30] E. Carrera, Theories and finite elements for multilayered, anisotropic, composite plates and shells, Archives of Computational Methods in Engineering 9 (2) (2002) 87–140.

[31] E. Carrera, Theories and finite elements for multilayered plates and shells: a unified compact formulation with numerical assessment and benchmarking, Archives of Computational Methods in Engineering 10 (3) (2003) 216–296.

[32] E. Carrera, G. Giunta, M. Petrolo, Beam Structures: Classical and Advanced Theories, John Wiley & Sons, 2011, DOI: 10.1002/9781119978565.

[33] E. Carrera, G. Giunta, P. Nali, M. Petrolo, Refined beam elements with arbitrary cross-section geometries, Computers and Structures 88 (5–6) (2010) 283–293, DOI: 10.1016/j.compstruc.2009.11.002.

[34] E. Carrera, M. Petrolo, E. Zappino, Performance of CUF approach to analyze the structural behavior of slender bodies, Journal of Structural Engineering 138 (2) (2012) 285–297, DOI: 10.1061/(ASCE)ST.1943-541X.0000402.

[35] E. Carrera, M. Petrolo, P. Nali, Unified formulation applied to free vibrations finite element analysis of beams with arbitrary section, Shock and Vibrations 18 (3) (2011) 485–502, DOI: 10.3233/SAV-2010-0528.

[36] E. Carrera, M. Petrolo, A. Varello, Advanced beam formulations for free vibration analysis of conventional and joined wings, Journal of Aerospace Engineering 25 (2) (2012) 282–293, DOI: 10.1061/(ASCE)AS.1943-5525.0000130.

[37] M. Petrolo, E. Zappino, E. Carrera, Refined free vibration analysis of one-dimensional structures with compact and bridge-like cross-sections, Thin-Walled Structures 56 (2012) 49–61, DOI: 10.1016/j.tws.2012.03.011.

[38] E. Carrera, S. Brischetto, Analysis of thickness locking in classical, refined and mixed multilayered plate theories, Composite Structures 82 (4) (2008) 549–562.

[39] K. J. Bathe, Finite element procedure, Prentice hall, 1996.

[40] E. Carrera, A. Pagani, M. Petrolo, Use of Lagrange multipliers to combine 1D variable kinematic finite elementsSubmitted.

[41] R. Courant, Differential and Integral Calculus, Interscience Publishers, 1937.

[42] G. Strang, Calculus, Welles-Cambridge Press, 1991.

[43] O. C. Zienkiewicz, R. L. Taylor, The Finite Element Method for Solid and Structural Mechanics, 6th Edition, Butterworth-Heinemann, Washington, 2005.

List of Table Captions

- (Tab. 1) Vertical displacement at points A and B on the free end of the cantilever I-section beam

- (Tab. 2) Vertical displacements, u_z, and normal stresses, σ_{yy}, at points A and B on the free and clamped ends, respectively. Reinforced plate undergoing a torsional-bending load

- (Tab. 3) Vertical displacements, u_z, at points A and B on the free end of the cylinder

- (Tab. 4) Normal stress component, σ_{yy}, at points A and B on the clamped end of the cylinder

- (Tab. 5) Vertical displacement, u_z, at the loaded point of the riveted I-section beam

Tables

	$-u_{z_A}$, mm	$-u_{z_B}$, mm	DOFs
$-u_{z_b} = \frac{F_z L^3}{3EI} = 0.951$, mm			
MSC Nastran models			
Solid	0.956	2.316	355800
Shell	1.006	(2.437)	61000
Classical and refined single-line models			
EBBM	0.951	0.951	93
TBM	0.964	0.964	155
$N = 1$	0.964	0.978	279
$N = 2$	0.956	0.978	558
$N = 3$	0.989	1.018	930
$N = 4$	0.989	1.287	1395
$N = 5$	0.993	1.481	1953
$N = 6$	0.992	1.462	2604
$N = 7$	0.997	1.560	3348
$N = 8$	0.997	1.851	4185

Present ML_{N_f, N_w}

N_f	N_w			
1	1	1.016	1.016	837
2	1	0.990	1.028	1116
2	2	0.951	1.940	1674
3	1	0.994	1.104	1488
3	2	0.950	1.984	2046
3	3	0.952	2.186	2790
4	1	0.983	1.201	1953
4	2	0.951	2.008	2511
4	3	0.954	2.197	3255
4	4	0.952	2.230	4185

Table 1: Vertical displacement at points A and B on the free end of the cantilever I-section beam

Model	$-u_{z_A}$, mm	$-u_{z_B}$, mm	σ_{yy_A}, MPa	σ_{yy_B}, MPa	DOFs
		MSC Nastran models			
Solid	1.297	1.163	4.041	1.955	469800
Shell/Beam	(1.393)	(1.265)	(4.194)	(2.542)	41400
		Classical and refined single-line models			
EBBT	1.233	1.233	3.368	3.310	93
TBM	1.233	1.233	3.368	3.310	155
$N = 1$	1.236	1.231	3.368	3.310	279
$N = 2$	1.223	1.175	4.009	2.901	558
$N = 3$	1.224	1.184	2.549	1.336	930
$N = 4$	1.239	1.187	2.530	1.236	1395
$N = 5$	1.245	1.187	2.790	1.359	1953
$N = 6$	1.256	1.181	3.176	1.537	2604
$N = 7$	1.261	1.178	3.313	1.734	3348
$N = 8$	1.270	1.166	3.313	1.734	4185
$N = 9$	1.276	1.167	3.714	1.710	5115

			Present ML_{N_p,N_s}			
N_p	N_s					
1	1	1.237	1.232	3.417	3.349	837
3	1	1.254	1.183	3.572	2.055	1488
3	3	1.278	1.161	3.475	1.447	2790
5	3	1.281	1.161	3.730	1.498	3813
5	5	1.281	1.160	3.753	1.500	5859
7	5	1.283	1.159	3.825	1.672	7254

Table 2: Vertical displacements, u_z, and normal stresses, σ_{yy}, at points A and B on the free and clamped ends, respectively. Reinforced plate undergoing a torsional-bending load

	Model		$-u_{z_A}$, mm	$-u_{z_B}$, mm	DOFs
			MSC Nastran models		
	Shell		1.062	0.412	20000
	Solid		1.066	0.409	100800
		Classical and refined single-line models			
	EBBT		0.583	0.583	93
	$N=3$		0.623	0.559	930
	$N=5$		0.807	0.452	1953
	$N=7$		0.941	0.383	3348
	$N=9$		0.997	0.392	5115
	$N=11$		1.039	0.377	7254

		Present $\text{ML2}_{N_t,N_b}$			
N_t	N_b				
1	1		0.589	0.588	558
3	1		0.594	0.588	1209
3	3		0.687	0.498	1860
5	1		0.684	0.581	2231
5	3		0.787	0.481	2883
5	5		0.868	0.431	3906
7	1		0.763	0.576	3627
7	3		0.809	0.483	4278
7	5		0.982	0.413	5301
7	7		0.989	0.395	6696
9	1		0.792	0.576	5394
9	3		0.967	0.462	6045
9	5		1.015	0.413	7068
9	7		1.016	0.401	8463
9	9		1.016	0.401	10230

				Present $\text{ML4}_{N_t,N_b,N_l,N_r}$		
N_t	N_b	N_l	N_r			
1	1	1	1	0.589	0.588	1116
1	1	3	3	0.592	0.587	2418
3	3	3	3	0.759	0.474	3720
3	3	5	5	0.827	0.476	5766
5	5	3	3	0.901	0.437	5766
5	5	5	5	0.968	0.414	7812
5	5	7	7	0.982	0.401	10602
7	7	5	5	1.017	0.404	10602

Table 3: Vertical displacements, u_z, at points A and B on the free end of the cylinder

Model	$\sigma_{yy} \times 10^{-5}$, Pa		DOFs
	pt. A	pt. B	
MSC Nastran models			
Shell	3.331	-3.729	20000
Solid	3.060	-3.409	100800
Classical and refined single-line models			
EBBM	3.243	-3.243	93
$N = 3$	3.723	-3.509	930
$N = 5$	3.187	-3.399	1953
$N = 7$	3.636	-4.188	3348
$N = 9$	3.868	-4.244	5115
$N = 11$	3.731	-4.033	7254
Present ML2$_{N_t,N_b}$			

N_t	N_b			
5	1	3.789	-3.244	2232
5	3	3.358	-3.550	2883
5	5	4.098	-4.196	3906
9	3	5.525	-4.400	6045
9	5	3.753	-3.892	7068
9	7	3.985	-3.702	8463
9	9	3.339	-3.776	10203

Present ML4$_{N_t,N_b,N_l,N_r}$

N_t	N_b	N_l	N_r			
1	1	1	1	3.247	-3.247	1116
3	1	1	1	3.920	-3.185	1767
3	3	3	3	3.507	-3.574	3720
5	3	3	3	2.875	-3.224	4743
5	5	5	5	3.614	-4.009	7812
7	5	5	5	3.936	-4.345	9207

Table 4: Normal stress component, σ_{yy}, at points A and B on the clamped end of the cylinder

Model	$-u_z$, mm		DOFs
	MSC Nastran model		
	CASE A	CASE B	
Solid	2.072	1.770	140800
	Classical and refined single-line models		
EBBM	0.803		93
TBM	0.814		155
$N = 3$	0.861		930
$N = 5$	1.097		1953
$N = 7$	1.122		3348
$N = 9$	1.353		5115

			Present $\mathrm{ML}_{N_f, N_w, N_s}$		
N_f	N_w	N_s			
			CASE A	CASE B	
1	1	1	0.937	0.841	1953
1	2	1	0.938	0.879	2232
2	2	1	1.451	1.120	2790
2	2	2	1.459	1.160	3906
2	3	2	1.488	1.187	4278
3	3	2	1.629	1.259	5022
3	3	3	1.896	1.376	6510
3	4	3	1.901	1.407	6975
4	4	3	1.905	1.412	7905
4	4	4	1.924	1.452	9765

Table 5: Vertical displacement, u_z, at the loaded point of the riveted I-section beam
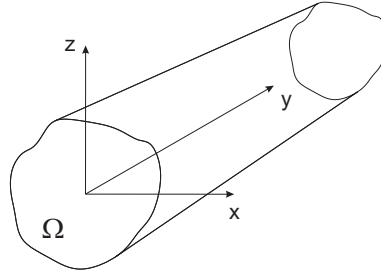
List of Figure Captions
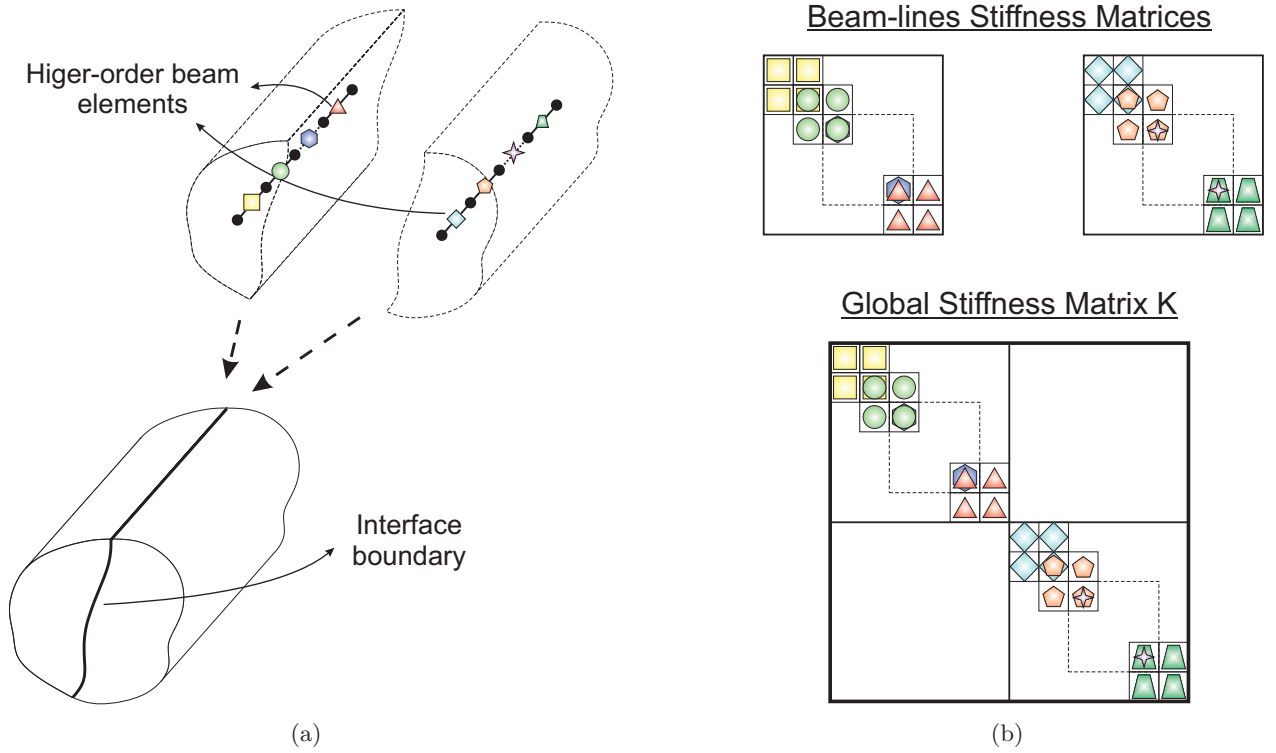
- (Fig. 1) Coordinate frame of the beam model

- (Fig. 2) Multi-line approach for the analysis of slender bodies (a) and assembly of the global stiffness matrix (b)
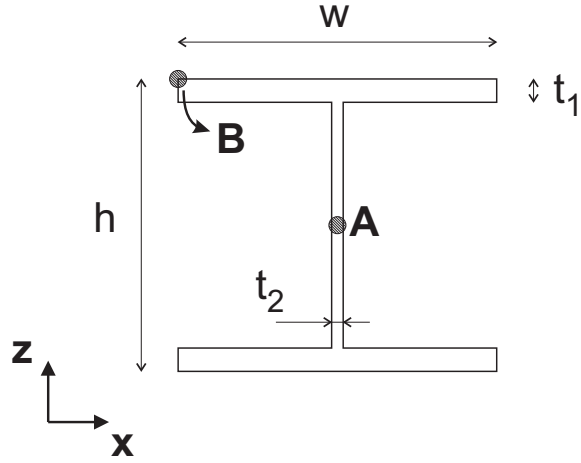
- (Fig. 3) I-section beam geometry and verification points

- (Fig. 4) Single- and multi-line approaches to the analysis of the I-section beam

    - (a) Single-line beam model

    - (b) Multi-line beam model

- (Fig. 5) Tip cross-section deformation of the I-section beam

- (Fig. 6) Normal stress distribution, σ_{yy}, at the clamped end of the I-section beam

    - (a) $\mathrm{ML}_{2,1}$

    - (b) $\mathrm{ML}_{3,2}$

    - (c) $\mathrm{ML}_{4,3}$

    - (d) Solid

- (Fig. 7) Cross-section of the reinforced plate. Dimensions are in millimeters

- (Fig. 8) Multi-line-beam approaches to the analysis of the reinforced plate

    - (a) Single-line model

    - (b) Two-line model

    - (c) Three-line model

    - (d) Four-line model

- (Fig. 9) Normal stress distribution, σ_{yy}, at the clamped end of the reinforced plate structure

    - (a) Single-line, $N = 2$

    - (b) $\mathrm{ML}_{1,1}$

    - (c) $\mathrm{ML}_{3,1}$

    - (d) $\mathrm{ML}_{3,3}$

Figures

Figure 1: Coordinate frame of the beam model

Figure 2: Multi-line approach for the analysis of slender bodies (a) and assembly of the global stiffness matrix (b)

Figure 3: I-section beam geometry and verification points
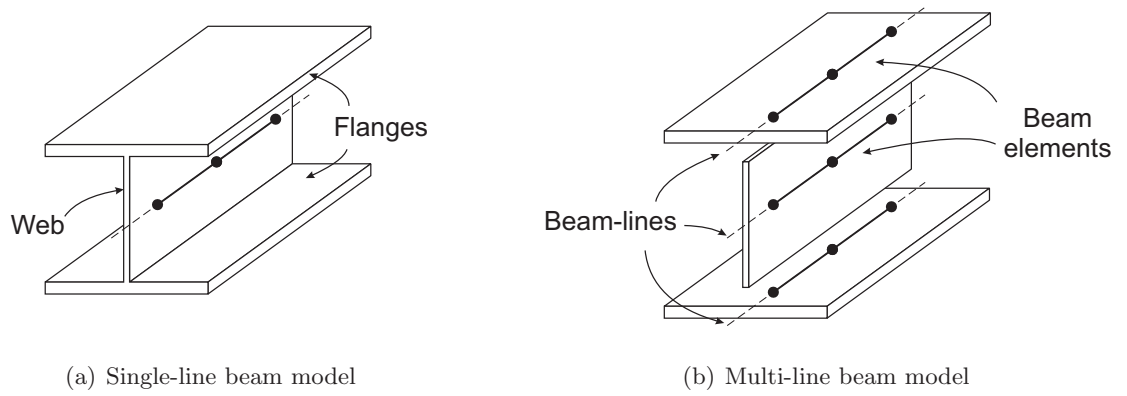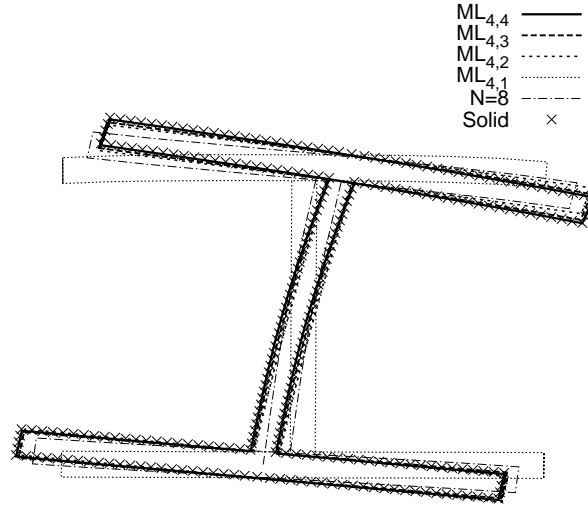

(a) Single-line beam model

(b) Multi-line beam model

Figure 4: Single- and multi-line approaches to the analysis of the I-section beam

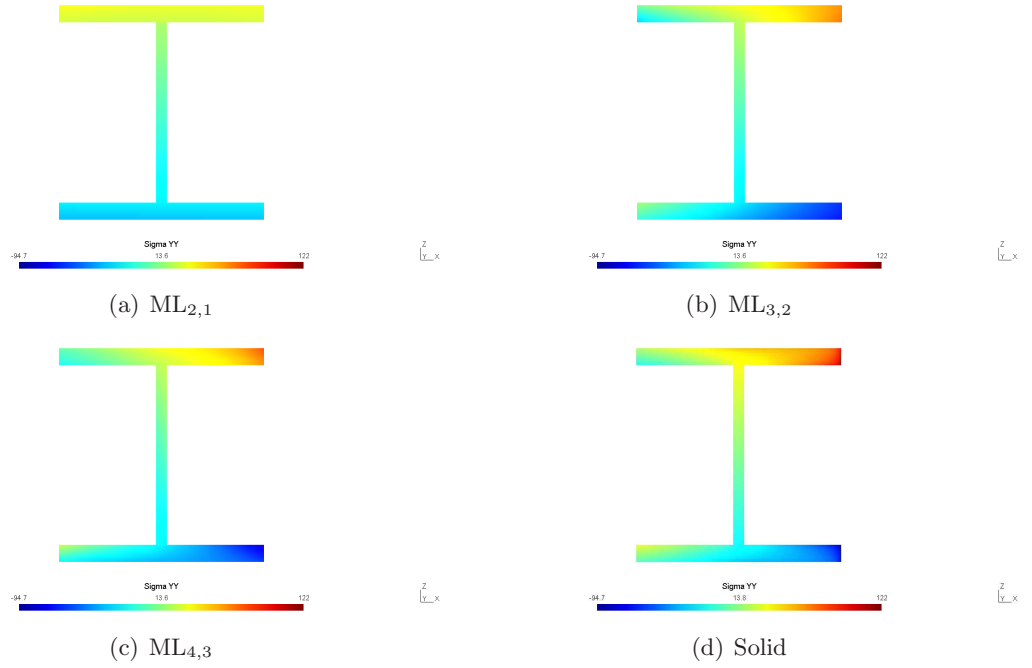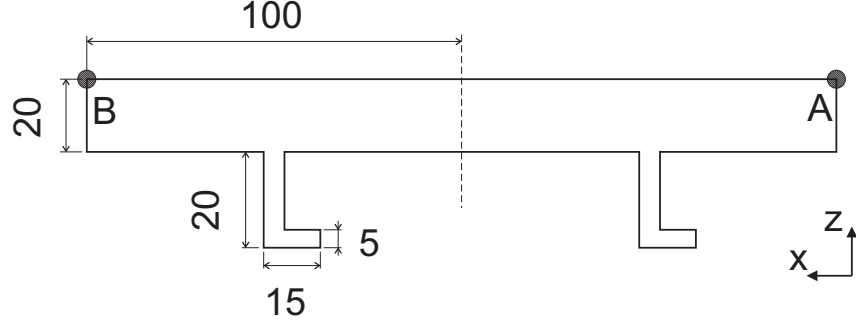Figure 5: Tip cross-section deformation of the I-section beam

(a) $ML_{2,1}$

(b) $ML_{3,2}$

(c) $ML_{4,3}$

(d) Solid

Figure 6: Normal stress distribution, σ_{yy}, at the clamped end of the I-section beam

Figure 7: Cross-section of the reinforced plate. Dimensions are in millimeters

(a) Single-line model

(b) Two-line model

(c) Three-line model

(d) Four-line model
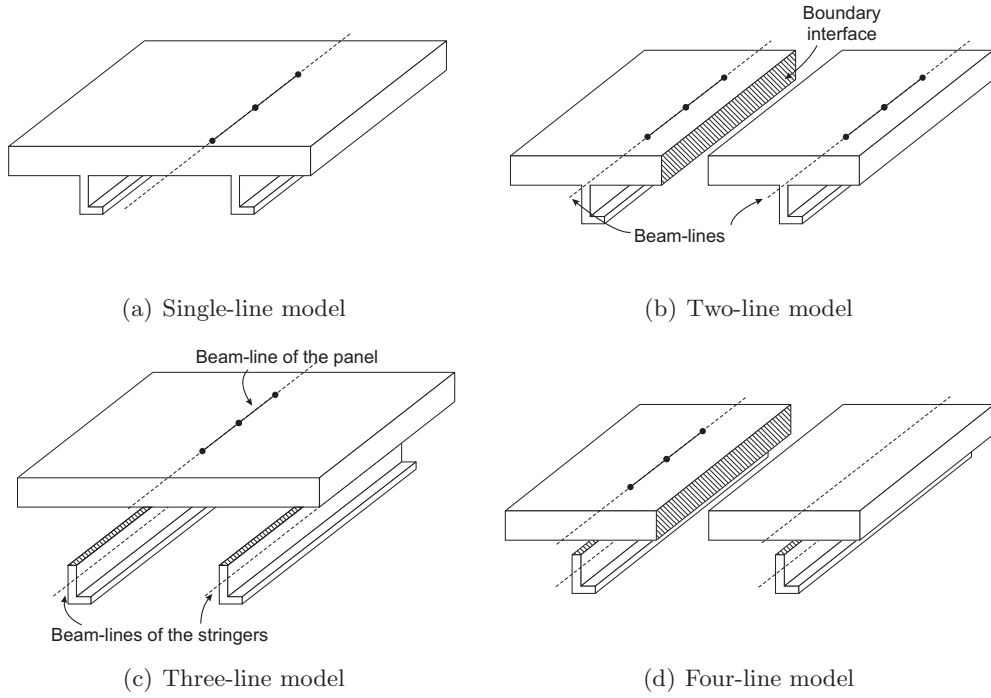
Figure 8: Multi-line-beam approaches to the analysis of the reinforced plate

(a) Single-line, $N = 2$

(b) $ML_{1,1}$

(c) $ML_{3,1}$

(d) $ML_{3,3}$

(e) Solid
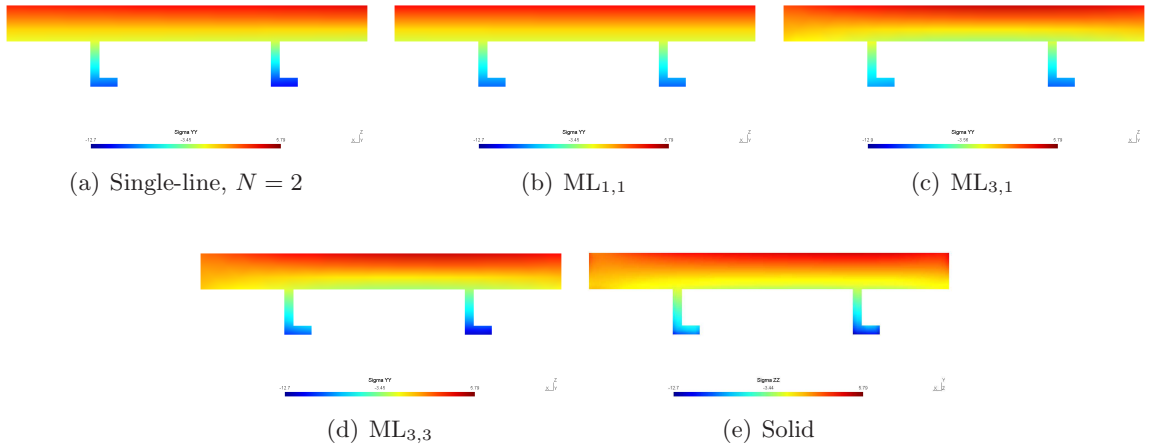
Figure 9: Normal stress distribution, σ_{yy}, at the clamped end of the reinforced plate structure
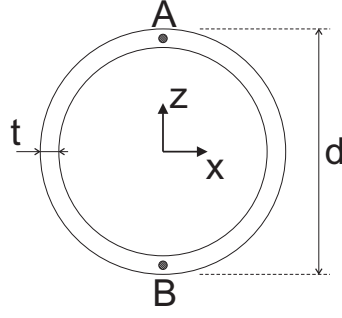
Figure 10: Cross-section of the thin-walled cylinder and verification points

(a) Single-line model   (b) Two-line model   (c) Four-line model
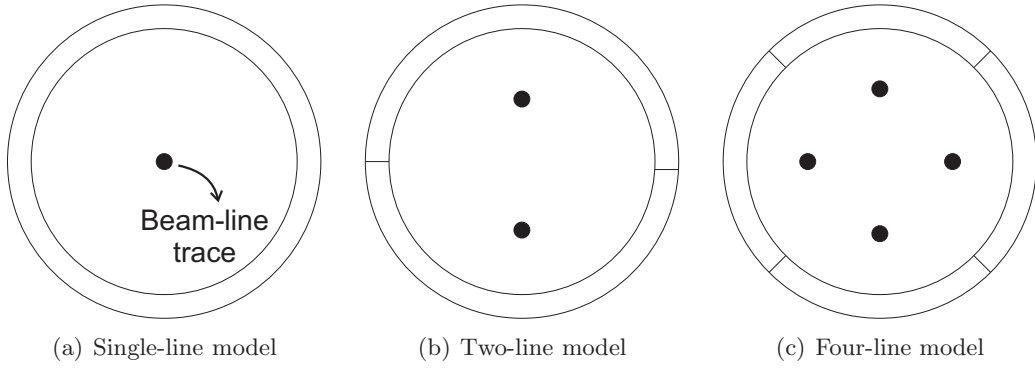
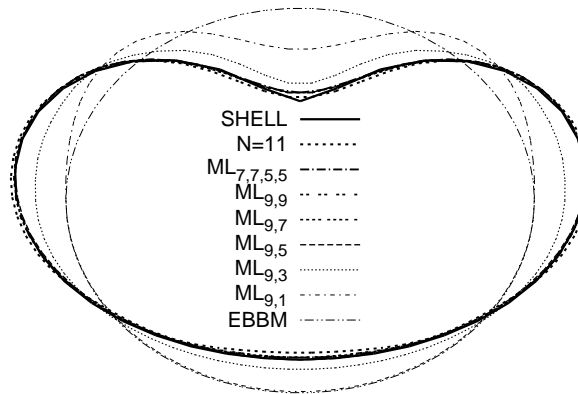Figure 11: Single- and multi-line beam models of the thin walled cylinder

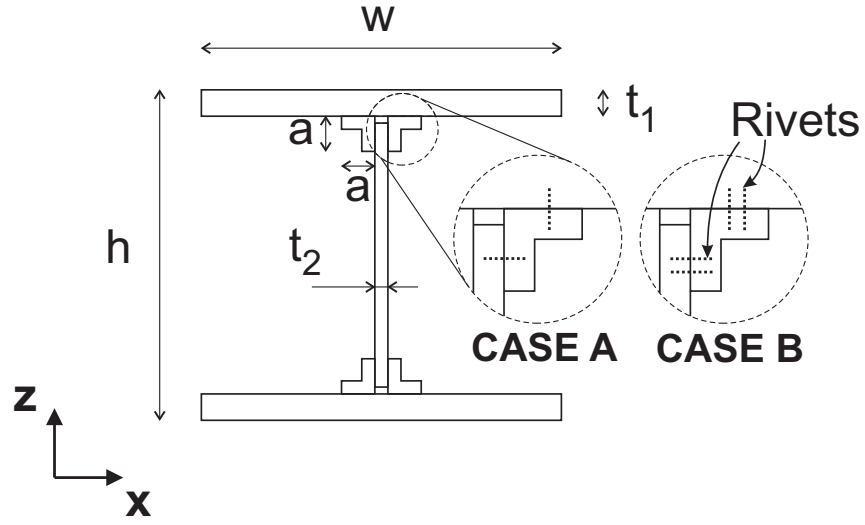Figure 12: Tip cross-section deformation of the thin-walled cylinder for different theories

Figure 13: Cross-section of the riveted I-section beam

(a) Single-line, $N = 9$

(b) $\text{ML}_{4,3,3}$, CASE A
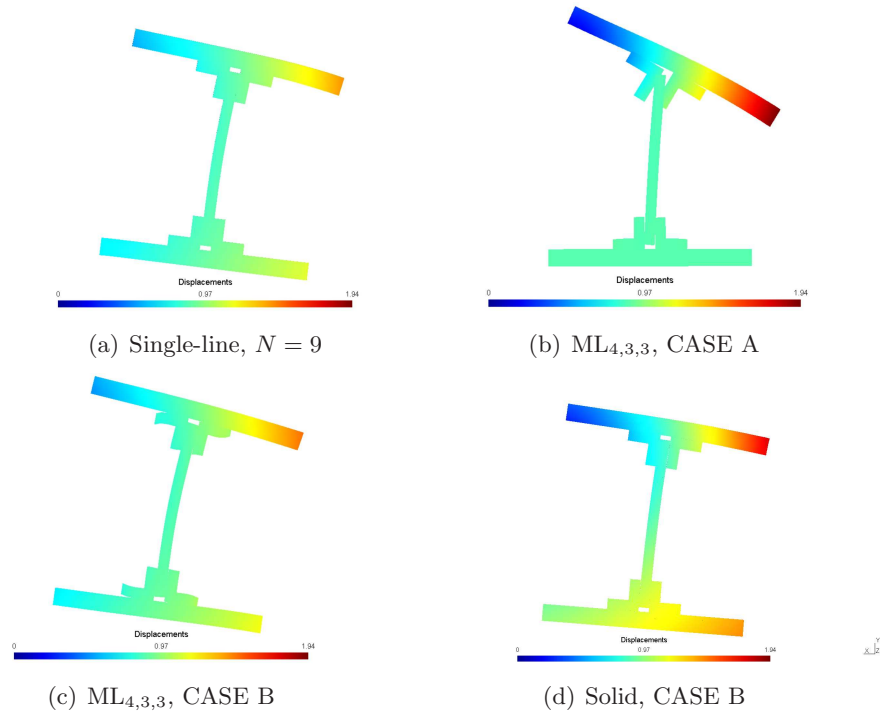
(c) $\text{ML}_{4,3,3}$, CASE B

(d) Solid, CASE B

Figure 14: Displacement field, $\sqrt{u_x^2 + u_y^2 + u_z^2}$, on the deformed tip cross-section of the riveted beam